Published in: Chemical Physics (2005), vol. 317, pp. 73-86
Status: Postprint (Author's version)

The vacuum UV photoabsorption spectrum of methyl bromide (CH_3Br) and its perdeuterated isotopomer CD_3Br: a Rydberg series analysis

R. Locht [a], B. Leyh [a], H.W. Jochims [b], H. Baumgärtel [b]

[a] *Laboratoire de Dynamique Moléculaire, Département de Chimie, Institut de Chimie, Bât. B6c, Université de Liège, Sart-Tilman par B-4000 Liège 1, Belgium*

[b] *Institut für Physikalische und Theoretische Chemie, Freie Universität Berlin, Takustraße 3, D-14195 Berlin, Germany*

Abstract

The vacuum UV photoabsorption spectrum of CH_3Br has been recorded between 6 and 25 eV. A large number of vibronic bands are observed. They were partly ascribed to vibrationless Rydberg transitions. In the high photon energy range of 12-25 eV, very weak diffuse bands are mostly assigned to transitions from the $3a_1$, le and ($2a_1$ + la_1) to 3s orbitals. In the 6-12 eV photon energy range, numerous weak to strong bands are observed. The sharpness is very variable over the entire spectral region. In a first step, the interpretation of the spectrum and the assignment of the Rydberg transitions is based on the simple Rydberg formula. The observed features are classified in two groups of four series, each converging to one of the two spin-orbit components of the $\tilde{X}\,^2E$ state of CH_3Br^+. Rydberg series of nsa_1, npa_1, npe, nd and possibly nf characters are observed. The same measurements have been made for the first time on CD_3Br in the 6-12 eV photon energy range. The observed features are classified into the same Rydberg series characterized by nearly the same δ values. Ionization energies for CD_3Br $\tilde{X}\,^2E_{3/2}$ at 10.565 eV and $\tilde{X}\,^2E_{1/2}$ at 10.902 eV are deduced. In a second step, we fitted the experimental data to an energy expression taking into account both the exchange interaction and the spin-orbit coupling. Already states with $n = 6$ are found to correspond to Hund's case (c). Constant values of the quantum defects are deduced.

Keywords: Photoabsorption; Rydberg series; CH_3Br; CD_3Br; Exchange interaction; Spin-orbit coupling

1. Introduction

The still topical and acute problem of the detrimental effects of the atmospheric pollutants is a main reason for the investigation of the organic halogenated compounds and particularly the various halogenated methanes.

Though bromine is a minor constituent in the Earth's atmosphere, its ozone depleting efficiency is estimated to be about 50-fold larger than that of chlorine [1]. Furthermore, bromocarbons have a high global warming potential [1, 2].

Methyl bromide, the largest reservoir of atmospheric bromine, is likely to contribute at least 50% of the organic bromine budget to the atmosphere [2]. It has both natural and anthropogenic sources. Since halons are being phased-out, methyl bromide has gained importance. However, the atmospheric lifetime of CH_3Br is estimated to be less than one year. Cessation of its emission would produce prompt results. These facts are strong incentives for the study of this compound.

In previous publications we extensively examined the vacuum UV spectroscopy, the photoelectron spectroscopy (TPES and He-I) and the mass spectrometric photoionization and electroionization of the halogenated derivatives of methane [3-9] and ethylene [10-17]. In many cases, the major importance of the localization and identification of neutral molecular states embedded in the ionization continua has been demonstrated [3-5, 9-11,13-17].

The polyhalogenated derivatives of methane have abundantly been studied in the last fifteen years [18-21] using almost all available spectroscopic techniques. The monosubstituted species received much less attention, and among them particularly CH_3Br. Its photoabsorption spectrum has been reported a few times, in the 180-110 nm wavelength region (40 000-90 000 cm^{-1}) and under different experimental conditions. To the

best of our knowledge, the photoabsorption spectroscopy of the perdeuterated isotopomer CD_3Br has been reported only once in the 185-158 nm wavelength region (54 000-63 300 cm^{-1}) [22].

The vacuum UV photoabsorption spectrum of CH_3Br was first reported by Price [23] in the wavelength region of 100-200 nm (6.2-12.4 eV) using a grazing incidence monochromator and the Lyman continuum as excitation source. The intensity is mainly confined to two types of electronic transitions, classified into two Rydberg series converging to the first two ionization limits at 10.49 and 10.80 eV, respectively. Two weaker series start at 66 020 and 68 680 $cm^{-1.}$

Hochmann et al. [24] and Felps et al. [22] studied the Rydberg transitions in the methyl halides CH_3Cl, CH_3Br and CH_3I. In the former work the authors analyzed the spectra on the basis of a linear correlation between the energy of the Rydberg transitions and the ionization energies. In the latter publication the authors restricted their study to the lowest s-type Rydberg transition in both the hydrogenated and perdeuterated methyl halides and presented vibrational assignments. In a later work, Felps et al. [25] reported the electronic spectra of the methyl and cyanogen halides without any detailed analysis of the methyl halides.

Causley and Russell [26] investigated the bromo-methanes in the 40 000-90 000 cm^{-1} region. By correlating Rydberg series in methyl bromide with corresponding series in Krypton the authors assigned transitions to 4d and 4f Rydberg orbitals. An analysis of the vibrational progressions in the 3s and 3p Rydberg states was also presented.

Despite a lower resolution in this energy range, the electron energy loss spectroscopy provides very useful information on molecular structure. The most recent well resolved (0.05 eV FWHM) dipole (e,e) measurements on CH_3Br were reported by Olney et al. [27] between 6 and 25 eV. They also derived the oscillator strength (related to the cross section and the extinction coefficient) for absorption of CH_3Br between 6 and 450 eV at low resolution (1 eV FWHM).

In the present contribution, we report on the photo-absorption spectrum of CH_3Br measured in the 6-25 eV photon energy range using synchrotron radiation. To the best of our knowledge, the photoabsorption spectrum of CD_3Br as observed between 6 and 12 eV photon energy, is reported for the first time. The aim of this paper is to reinvestigate in detail the vibrationless Rydberg transitions in CH_3Br and CD_3Br. An extensive vibrational analysis is presented in the companion paper.

2. Experimental

2.1. Experimental setup

The experimental setup used in this work has already been described in detail elsewhere [14]. Only the most salient features will be reported here.

Synchrotron radiation available from the BESSY I facility (Berlin, Germany) is dispersed with a modified vacuum UV normal incidence 225 McPherson monochromator with a focal length of 1.5 m, instead of 1 m in the commercial version (lm-NIM-2 beamline). A laminar Zeiss grating is used for the efficient reduction of the second spectral order. It is gold coated with 12001/mm and its transmission breaks down above 26 eV (210 000 cm^{-1} or 47 nm). The width of the entrance and exit slits of 100 μm ensures a 0.1 nm wavelength resolution corresponding to a resolving power of about 1200 at 10 eV.

Recently, the 3m-NIM-2 beamline at the BESSY II facility (Berlin, Germany) has been started [28]. This monochromator is equipped with a platinum grating of 2400 1/mm and its transmission is optimal between 10 and 40 eV (124-31 nm). The entrance and exit slits were adjusted between 25 and 50 μm leading to a resolving power of 25 000-12 600 at 10 eV (124 nm) photon energy. This monochromator was used for recording well defined restricted photon energy regions at high resolution.

In both setups, the light passes through a 1 mm thick stainless steel microchannel plate necessary to maintain a differential pressure of 1:1000 before entering a 30 cm long stainless steel absorption cell. Most spectra are recorded without filter on the light path. However, in some cases a LiF filter (cutoff at 11.8eV or 95 000 cm^{-1} or 105 nm) is used, which can be inserted in the light beam without vacuum breakdown. The vapor pressure in the cell is measured by a Balzers capacitor manometer. The light is detected by a sodium salicylate sensitized photomultiplier located at the end of the absorption cell and in front of the absorption cell entrance slit. Output pulses are recorded by a 100 MHz counter. The recording of an absorption spectrum requires one scan with gas in the absorption cell and one with the empty cell. The stability of the synchrotron radiation and of the pressure in the cell ensured reliable absorption data. When necessary, the spectra presented in the following

sections are corrected for any pressure drift. The commercially available CH_3Br, purchased from Praxair and of 99.5% purity, was used without further purification. CD_3Br, purchased from Merck, Sharp and Dohme, is certified at 99 at.% purity. No noticeable impurity was observed by mass spectrometry at 21.2 eV photon energy. Therefore, the sample was used without further purification.

2.2. Data handling and error estimation

As will be mentioned in the next section, in the high photon energy part of the absorption spectrum weak and diffuse structures are superimposed on an intense continuum. To make the characterization of these features easier, a continuum subtraction procedure has been applied. This has already been used successfully in previous spectral analysis [6,29]. For this purpose, the experimental curve is severely smoothed to simulate the underlying continuum which is then subtracted from the original photoabsorption spectrum. The smoothing procedure consists in filtering the experimental curve by fast Fourier transform. The weak features emerge then from a remaining strongly attenuated background.

The wavelength calibration of the 1.5m-NIM mono-chromator has been performed by using the Ar^+ absorption spectrum between the $^2P_{3/2}$ and the $^2P_{1/2}$ ionic states. The accuracy of this calibration is better than 2 meV. In the measurements between 6 and 25 eV photon energy, the photoabsorption spectrum has been recorded with an energy interval of about 10 meV. The error on the energy position of a feature is estimated to be 15meV. In the photoabsorption spectra between 6 and 12 eV, an energy increment of 1.5 meV has been adopted. The error on the energy position of a feature is estimated to be of the order of 4 meV. This evaluation is confirmed by the reproducibility of energy positions measured in four different spectra recorded in a two year interval. For high resolution spectra recorded with the 3m-NIM monochromator 50-200 meV photon energy ranges were scanned with 50-200 μeV energy intervals.

3. Experimental results

3.1. The CH_3Br photoabsorption spectrum

The photoabsorption spectrum of CH_3Br has been measured between 6 and 25 eV photon energy. A typical coarse recording (with energy interval of 10 meV) is reproduced in Fig. 1(a) where the molar extinction coefficient $\varepsilon_{h\nu}$ is plotted as a function of the photon energy. Particular attention has been devoted to the energy range of 11-25 eV where the subtraction procedure (see Section 2.2) has been applied to enhance the weak bands. The result is shown in Fig. 1(b). To help visualizing the structures, a FFT-smoothed curve has been drawn through the data points. The energy positions of these weak bands are listed in Table 1 together with the proposed assignments.

Energy positions estimated from the dipole (e,e) cross section curve as reported by Olney et al. [27] are inserted in this table. The convergence limits listed in this table are those reported by Olney et al. [27], Karlsson et al. [30], Von Niessen et al. [31] and those measured in our laboratory [32] by synchrotron radiation [33] and by fixed wavelength He(I) and He(II) photoelectron spectroscopy, respectively.

The fine structure energy region, recorded between 6 and 12eV with the 1.5m-NIM monochromator, and with energy increments of 1.5meV, is shown in Fig. 2.

In the same figure the assignment of the main features to series of vibrationless Rydberg transitions has been inserted. The convergence limits are the ionization energy values determined by Karlsson et al. [30] using He(I) photoelectron spectroscopy.

3.2. The CD_3Br photoabsorption spectrum

The photoabsorption spectrum of CD_3Br has been recorded between 6 and 12 eV photon energy (Fig. 3). The assignments of the vibrationless Rydberg transitions are inserted in this figure with convergence limits from an ongoing photoelectron spectroscopic work [32].

4. Discussion of the experimental data

For clarity in the following discussion, let us remind that the molecular orbital configuration of CH_3Br in the C_{3v} point group is:

Published in: Chemical Physics (2005), vol. 317, pp. 73-86
Status: Postprint (Author's version)

$$Br(ls^2 2s^2 2p^6)C(ls^2)Br(3s^2 3p^6 3d^{10}),$$

$$(la_1)^2(2a_1)^2(le)^4(3a_1)^2(2e)^4:\ \tilde{X}\ ^1A_1,$$

where the first atomic-like orbitals correspond to the inner-shell orbitals which are localized on the Br and C atoms. The la_1 and $2a_1$ are inner-valence molecular orbitals whereas the le, $3a_1$ and 2e molecular orbitals have outer-valence character. The most accurate and well-resolved He(I) photoelectron spectrum [30] provides the adiabatic ionization energies at 10.543 ± 0.006 eV ($2e^{-1}$), 13.0 eV ($3a_1^{-1}$) and at 14.5 eV ($1e^{-1}$) successively. The lowest ionic state shows a $^2E_{3/2}$-$^2E_{1/2}$ spin-orbit splitting of 319 ± 12meV (2573 ± 96 cm^{-1}) [30]. It has to be pointed out here that the spin-orbit interaction energy in the free Br atom is 0.457 eV (3685 cm^{-1}) [36].

Fig. 1. *(a) Vacuum UV photoabsorption spectrum of CH_3Br in the 6-25 eV photon energy range. The successive ionization continua are indicated, (b) Intensity difference Δ between the photoabsorption spectrum (PAS) and the strongly smoothed photoabsorption spectrum (SSPA) plotted as a function of the photon energy in the 12-24 eV range. The continuous curve is the result of a FFT smoothing. The assignments of the structures and ionization continua are indicated by vertical bars.*

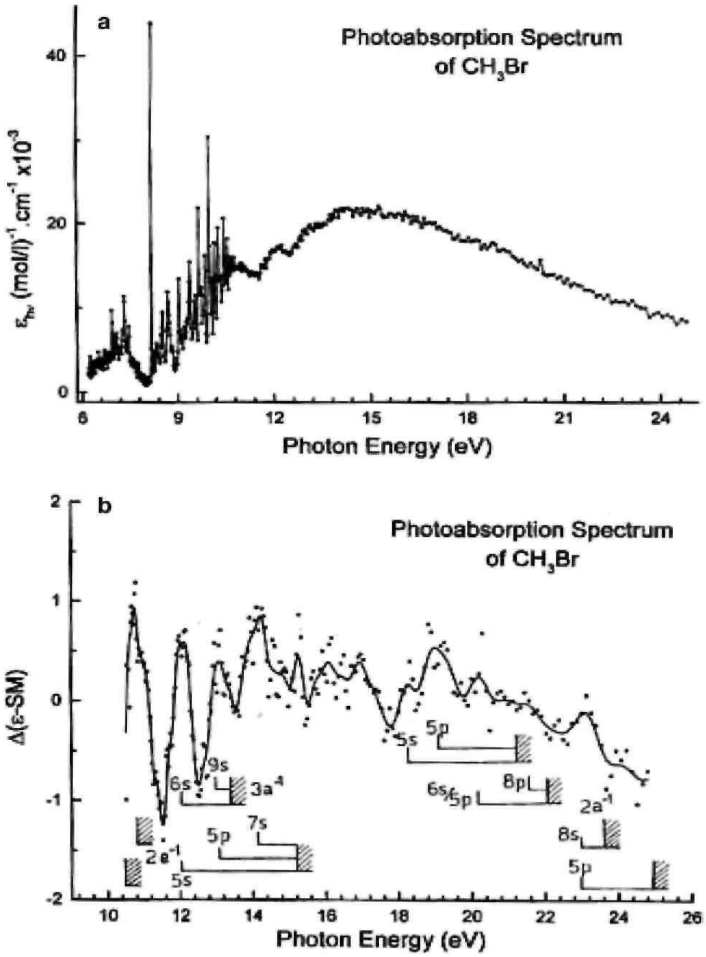

Higher lying vertical ionization energies are located at 13.5 eV *($3a_1^{-1}$)* and 15.0-15.7 eV ($1e^{-1}$) [30]. With the He(II) resonance line at 30.4 nm, vertical ionization energies are measured at 21.2 eV ($2a_1^{-1}$) and at 22.0 eV ($1a_1^{-1}$) [31]. Olney et al. [27] measured vertical ionization energies at 21.3, 22.0, 23.6, 24.9 and at 27.8 eV and above 30 eV in the photoelectron spectra recorded with 34 and 70 eV photons produced by synchrotron radiation. These ionization energies were assigned to many body ion states resulting from the $(2a_1 + 1a_1)^{-1}$ and the $1a_1^{-1}$ ionizations [27, 33].

4.1. The Rydberg series analysis

As clearly appears from the photoabsorption spectrum of CH_3Br reproduced in Fig. 1, two distinct parts show up: (i) the low energy part extending from 6 to 11 eV and with an abundant fine structure and (ii) the high

Published in: Chemical Physics (2005), vol. 317, pp. 73-86
Status: Postprint (Author's version)

energy part spread over the 12-25 eV photon energy range, made of weak and broader bands. For the assignment of the features observed in this spectrum, their energy positions E_{Ryd} were first fitted to the Rydberg formula

$$E_{\mathrm{Ryd}} = \mathrm{I.E.} - \frac{R}{(n-\delta)^2} = \mathrm{I.E.} - \frac{R}{n^{*2}}, \qquad (1)$$

Fig. 2. *Vacuum UV photoabsorption spectrum of CH_3Br in the 6-12 eV photon energy range. The main vibrationless Rydberg transitions and their respective convergence limit are indicated by vertical bars.*

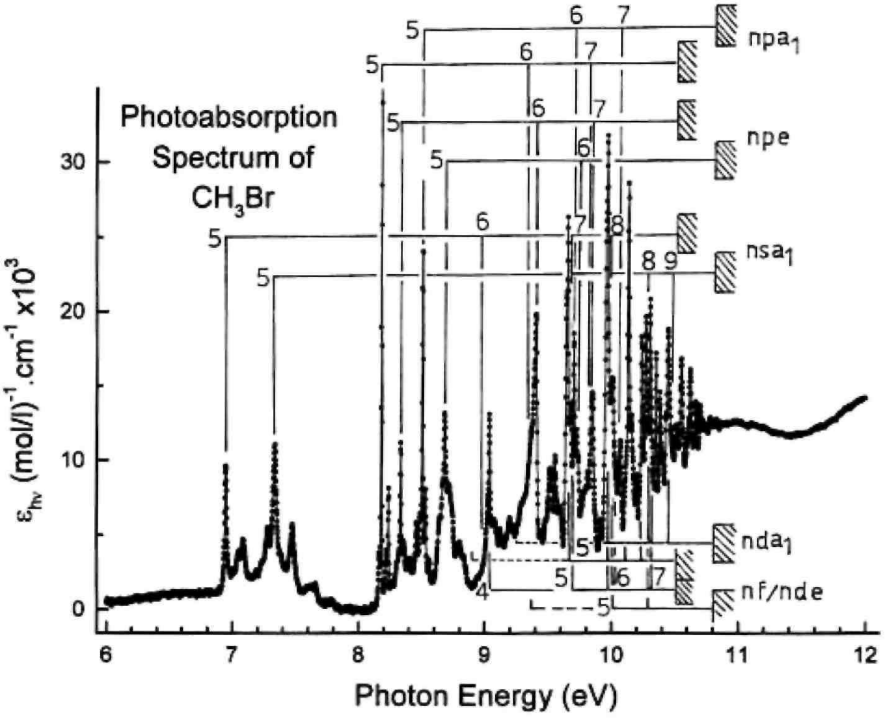

Fig. 3. *Vacuum UV photoabsorption spectrum of CD_3Br in the 6-12 eV photon energy range. The main vibrationless Rydberg transitions and their respective convergence limit are indicated by vertical bars.*

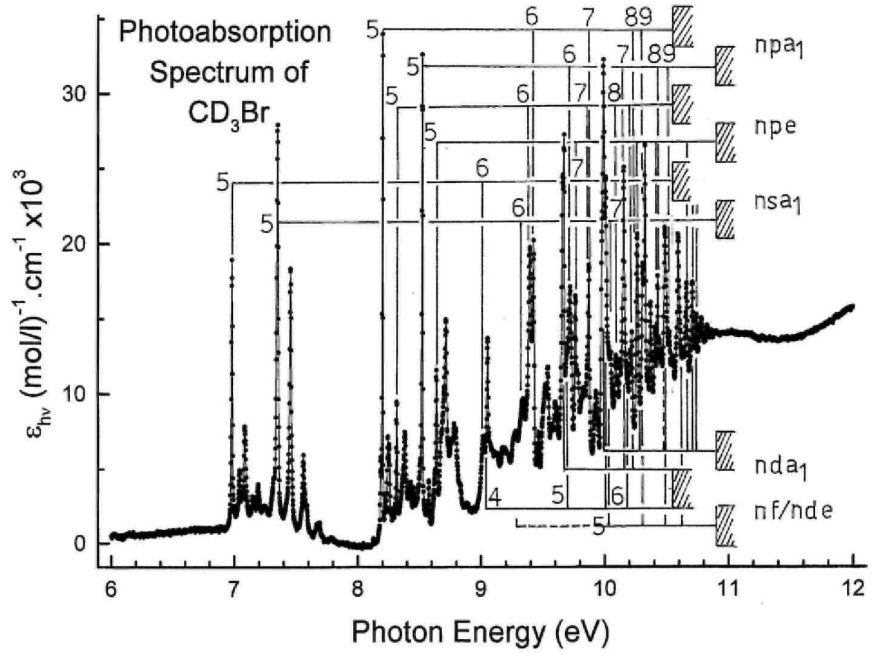

Published in: Chemical Physics (2005), vol. 317, pp. 73-86
Status: Postprint (Author's version)

Table 1: *Energy positions (eV) of the Rydberg transitions in the CH_3Br photoabsorption spectrum as defined by their band maxima in the 11-25 eV photon energy range*

Band maxima		Conversion limit (eV)	Assignment
This work	**[27][a]**	**[27,30-32][b]**	***n*** - Rydb. trans.*
12.1	12.12	13.5/13.5/13.5 - $3a_1^{-1}$	3.117 - $3a_1 \rightarrow 6s$
		15.0/15.4/15.1 - $1e_{3/2}^{-1}$	2.166 - $1e_{3/2} \rightarrow 5s$
13.1	13.10	13.5/13.5/13.5 - $3a_1^{-1}$	2.030-5.832 - $3a_1 \rightarrow 9s$
		15.0/15.4/15.1 - $1e_{3/2}^{-1}$	2.675 - $1e_{3/2} \rightarrow 5p$
14.2	14.0	15.0/15.4/15.1 - $1e_{3/2}^{-1}$	2.432-3.890 - $1e_{3/2} \rightarrow 7s$ 3.235 - $1e_{3/2} \rightarrow 6s$
		15.7/15.7/15.7 - $1e_{1/2}^{-1}$	2.916- $1e_{1/2} \rightarrow 5s$
15.3	15.2	15.7/15.7/15.7 - $1e_{1/2}^{-1}$	5.216- $1e_{1/2} \rightarrow 8s$
16.1-16.9	15.6-17.1	(17.9-19.7)	$? \rightarrow 5s$
18.2	17.9	21.3/21.2-$(2a_1 + 1a_1)^{-1}$	2.046 - $2a_1 + 1a_1 \rightarrow 5s$
19.0	18.6	22.1/22.0-$(2a_1 + 1a_1)^{-1}$	2.459 - $2a_1 + 1a_1 \rightarrow 5p$
			2.265 - $2a_1 + 1a_1 \rightarrow 5s$
20.2	20.6	22.1/22.0 -$(2a_1 + 1a_1)^{-1}$	2.712-$2a_1 + 1a_1 \rightarrow 5p$
			3.063 - $2a_1 + 1a_1 \rightarrow 6s$
21.6	-	22.1/22.0-$(2a_1 + 1a_1)^{-1}$	5.498 - $2a_1 + 1a_1 \rightarrow 8p$
		23.6-$(2a_1 + 1a_1)^{-1}$	2.608 - $2a_1 + 1a_1 \rightarrow 5p$
23.1		23.6-$(2a_1 + 1a_1)^{-1}$	5.216-$2a_1 + 1a_1 \rightarrow 8s$
		24.9 -$(2a_1 + 1a_1)^{-1}$	2.749 - $2a_1 + 1a_1 \rightarrow 5p$
		27.8 -$(2a_1 + 1a_1)^{-1}$	-
		>30 - $1a_1^{-1}$	-

Convergence limits data refer to the vertical ionization energy (IE_V) values (eV). [a] For explanation, see text. [b] In many body ion states the dominant character of the configuration is given by a bold case.

where the Rydberg constant it R = 13.60569 eV [34], δ is the quantum defect, n^* is the effective principal quantum number and I.E. is the convergence limit of the Rydberg series. When the principal quantum number is mentioned, e.g. in Table 1, its lowest value is conventionally taken to be $n = 5$ as in Kr.

A more appropriate formula taking into account both exchange (singlet-triplet splitting) and spin-orbit coupling will be used in a second step of our analysis for the Rydberg series converging to the $(2e)^{-1}$ continuum.

The $2e \rightarrow n\ell$ excitation provides among others ^3E and ^1E Rydberg states. Additionally, both states undergo the Jahn-Teller splitting. This latter effect is evaluated in the companion paper and is shown to be small (36 meV stabilization energy).

4.2. The high energy region

As far as the high energy part of the photoabsorption spectrum of CH_3Br is concerned, the data obtained in the present work are listed in Table 1 together with the only available literature data [27]. These data were obtained by also handling the dipole (e,e) oscillator strength spectrum of CH_3Br [27] using the subtraction procedure described in Section 2.2. A reasonable agreement is found between both experiments. However, no assignments have been proposed in the literature. Tentative assignments are proposed in the third column of Table 1 together with associated effective principal quantum numbers.

The broad band extending over the 16-17 eV region is observed in both experiments. It could correspond to a 5s Rydberg state, characterized by $n^* = 2.00$, if a convergence limit at 19.9 eV is assumed. No such ionic state of CH_3Br^+ has been mentioned in the literature. We recently investigated the threshold photoelectron spectrum (TPES) of this molecule between 10 and 30 eV photon energy by using synchrotron radiation as a tunable excitation source [35]. Weak TPES-bands are detected at 17.9, 18.8, 19.7 and 21.32 eV. Their intensity ratio with respect to the 21.3 eV band is 0.3/0.26/0.14/ 1.00, respectively. A shoulder, not resolved in the dipole (e,e) work [27], is observed at 20.4 eV. Transitions to doubly excited ion states could account for the weakness of these bands in the TPES. The weak and broad signals present in the photoabsorption spectrum could be involved in the autoionization of Rydberg states to (nearly) resonant ionic states. The Rydberg

states at 16-17 eV could also be able to play a role in resonant dissociative autoionization as it is the case for the CH_3^+ ion production from CH_3F [5], CH_3Cl [9] and for the $C_2H_3^+$ fragment from C_2H_3Br [15]. This investigation is still in progress.

4.3. The low energy region: Analysis using the Rydberg equation (1)

The vibrationless Rydberg series observed for CH_3Br between 6 and 12 eV are shown in Fig. 2 and their energy positions and assignments are listed in Table 2. In a first step the transitions have been classified according to the nature of the involved Rydberg orbital and by gathering both $^2E_{3/2}$ and $^2E_{1/2}$ spin-orbital components. This classification is based upon the value of the effective principal quantum numbers n^*. Energy levels corresponding to several possible assignments are listed in square brackets. Two previous data sets [24,26] have been included for comparison with the assignments proposed by these authors. As mentioned earlier, the estimated error on the present measurements is about 4meV or 30 cm^{-1}. No error estimation being provided by the latter authors, any further critical comparison is made difficult. However, as shown in Table 2, for most of the levels, the correspondence between the three measurements is univocal.

Obviously, the best agreement is found between the present measurements and the data published by Caus-ley and Russell [26]. For the assignments deduced in the present work, and listed in Table 2, the most accurate abiabatic ionization energies (IE_{ad}) of CH_3Br as reported by Karlsson et al. [30], i.e. $IE_{ad}(\tilde{X}\,^2E_{3/2}) = 10.543 \pm 0.006$ eV and $IE_{ad}(\tilde{X}\,^2E_{1/2}) = 10.862 \pm 0.006$ eV, have been used.

Concerning the $2e \rightarrow nsa_1$ Rydberg series, for both spin-orbit components average quantum defects of respectively, $\delta = 1.067$ and 1.032 have been determined with a standard deviation of 0.045. However, the quantum defect varies slowly with the principal quantum number n because of the relative evolution of the exchange versus spin-orbit interactions with n. This will be dealt with later in this paper. Though n^* values agree well with each other within the standard deviation, a propensity of differentiation of the ($^2E_{3/2}$)-nsa_1 and the ($^2E_{1/2}$)-nsa_1 Rydberg states seems to arise. Within one series the variation of δ is rather random. For CH_3C1 [7] a more monotonic δ variation with n was observed.

The corresponding assignments basically agree with those proposed by Hochmann et al. [24] and Causley and Russell [26]. These authors used 10.541 and 10.856 eV [24] and 10.540 and 10.859 eV [26] for both adiabatic ionization IE_{ad}, respectively. In Table 2 several energy levels listed in square brackets correspond to alternative possible assignments. Particularly in the ($^2E_{1/2}$)-nsa_1 series the assignment of the transitions observed at 85 329, 85 833 and 86 253 cm^{-1} are less obvious. Furthermore, as shown in Table 2, the 75 643 cm^{-1} [24] or 74 684 cm^{-1} [26] bands are not de tected in the present work. These were both assigned to a $2e \rightarrow 6sa_1$ transition, Rydberg series converging to the $^2E_{1/2}$ ionic state [24,26]. In this region the signal is close to background in our spectrum where, however, bands are observed at 9.372 eV (75 590 cm^{-1}) and 9.405 eV (75 856 cm^{-1}) (see Table 2). Their corresponding effective quantum numbers n^* deduced from Eq. (1) are not compatible with ns-type Rydberg transitions.

As observed for CH_3Cl [7], the CH_3Br photoabsorption spectrum is dominated by np-type Rydberg transitions. Due to the non-spherical character of the molecular field, the three p orbitals are split into one a_1 and one e orbital. These Rydberg orbitals are respectively aligned along and perpendicularly to the C_{3v} symmetry axis of the molecule. This distinction has not been mentioned earlier [24,26], though both transitions behave quite differently, with quantum defects equal to $\delta = 0.588$ (0.579) and 0.543 (0.533) for the $2e \rightarrow npa_1$ and the $2e \rightarrow npe$ transitions, respectively. Values in parenthesis correspond to the series converging to $\tilde{X}\,^2E_{1/2}$. This explains discrepancies between Causley and Russell's [26] assignments and those proposed in this work.

Except for the energy levels at 10.416 and 10.454 eV (see Table 2) the $2e \rightarrow npa1$ series converging to the $^2E_{3/2}$ and $^2E_{1/2}$ ionic states could be characterized by an average quantum defect $\delta = 0.588 \pm 0.034$ and 0.579 $\pm$ 0.030 using the simplified Eq. (1). This classification agrees well with the assignments proposed in both previous works [24, 26]. The authors also mentioned the remarkably constant value of 0.55 of the quantum defect [24]. To support their assignments both authors used correlations between Rydberg transition energies in the CH_3Br molecule and the Kr atom.

Hochmann et al. [24] correlated $2e \rightarrow nsa_1$ and $2e \rightarrow npa_1$ transitions to series converging to the $^2E_{3/2}$ and $^2E_{1/2}$ ionic states based on the constancy of (i) the energy difference, i.e. nearly the $^2E_{3/2}$-$^2E_{1/2}$ spin-orbit splitting, and (ii) the difference between the effective principal quantum number values $\Delta n^* \approx 1$.

Causley and Russell [26] correlated the term values T_n of ns and np series in CH_3Br and Kr. They measured the ΔT_n and observed a remarkable convergence of $\Delta T_n \rightarrow 0$ between CH_3Br and Kr for high n values. However, this correlation was less convincing for the np series

Published in: Chemical Physics (2005), vol. 317, pp. 73-86
Status: Postprint (Author's version)

***Table 2** : Vibrationless Rydberg transitions as observed for CH_3Br in the present work and in previous reports [24] and [26] for both spin-orbit components: parts (a) and (b) converge to the $^2E_{3/2}$ and $^2E_{1/2}$ ionic states, respectively*

This work				Literature Data	
E_{Ryd} (eV)	E_{Ryd}(cm^{-1})	n^*	E_{Fit} (eV)	[24]	[26]
		1. 2e → nsa_1			
		Part (a)			
6.944	56 010	1.944	6.943	56 062	56 023
8.974	72 383	2.945	8.980	73 035	72 152
9.667	77 969	3.941	9.672	77 985	77 871
9.990	80 575	4.960	9.988	80 548	80 511
10.152	81 881	5.899	10.159	81927	81 879
10.261	82 761	6.946	10.262	-	82 715
[10.328][a]	83 301	7.955	10.328	-	83 266
-	-	-	-	-	83 621
10.404	83 914	9.858	10.406	-	-
10.430	84 124	10.973	10.430	-	-
		Part (b)			
7.332	59 137	1.963	7.331	59 207	59 158
-	-	-	-	75 643	74 684
9.997	80 634	3.967	9.992	80 548	80 427
10.312	83 472	4.974	10.308	83 070	82 997
10.480	84 527	5.968	10.478	84 459	84 405
[10.579][a]	85 329	6.934	10.581	-	85 268
[10.642][a]	85 833	7.864	10.647	-	85 832
[10.694][a]	86 253	8.999	10.692	-	86 209
10.725	86 503	9.963	10.725	-	-
10.751	86 713	11.071	10.749	-	-
		2. 2e → npa_1			
		Part (a)			
8.179	65 972	2.399	8.181	66 058	66 730
9.372	75 590	3.409	9.367	75 872	75 702
9.846	79 413	4.418	9.841	79 554	79 470
10.077	81276	5.403	10.077	81 300	81 317
10.210	82 349	6.392	10.211	-	82 374
[10.296][a]	83 043	7.422	10.295	-	83 035
[10.391][a]	83 809	9.461	10.389	-	-
[10.416][a]	84 010	10.350	10.417	-	-
10.454	84 317	12.364	10.454	-	-
[10.468][a]	84 430	13.467	10.467	-	-
10.478	84 511	14.468	10.477	-	-
		Part (b)			
8.508	68 621	2.404	8.508	68 719	69 306
9.685	78 115	3.400	9.687	78 431	78 368
[10.165][a]	81986	4.418	10.160	82 102	82 046
[10.391][a]	83 809	5.375	10.396	83 977	83 893
[10.528][a]	84 914	6.382	10.530	-	84 950
10.616	85 624	7.437	10.614	-	-
10.709	86 374	9.430	10.708	-	-
		3. 2e → npe			
		Part (a)			
8.335	67 226	2.482	8.329	67 304[c]	67 246[c]
9.405	75 856	3.458	9.423		
9.857	79 502	4.454	9.867		
10.083	81 325	5.439	10.091		
10.218	82 414	6.470	10.220		
[10.296][a]	83 043	7.421	10.300		
10.358	83 543	8.553	10.357		

Table 2 *(continued)*

This work				Literature Data	
E_{Ryd} (eV)	E_{Ryd} (cm^{-1})	n^*	$\pounds_{Fit}$ (eV)	[24]	[26]
[10.391][a]	83 809	9.461	10.392		
[10.416][a]	84 011	10.350	10.419		
10.438	84 188	11.383	10.440		
[10.468][a]	84 430	13.467	10.468		
		Part (b)			
8.684	70 041	2.499	8.680	70 161[c]	70 083[c]
9.744	78 591	3.488	9.746		
-	-	-	-		
-	-	-	-		
-	-	-	-		
10.623	85 680	7.545	10.619		
10.675	86 100	8.530	10.673		
10.711	86 390	9.492	10.711		
10.738	86 608	10.475	10.738		
10.758	86 769	11.438	10.759		
10.777	86 922	12.652	10.775		
		4. 2e → nd(a_1)			
		Part (a)			
(8.947)[b]	72 162	2.920	8.942	67 304	70 083
9.659	77 905	3.923	9.656		
9.980	80 494	4.916	9.980		
10.139	81776	5.803	10.145		
10.250	82 672	6.814	10.248		
[10.328][a]	83 300	7.955	10.326		
		Part (b)			
[9.256][a]	74 655	2.917	9.261	70 161	72 957
9.975	80 454	3.916	9.975		
10.311/314	83 164/188	4.969	10.312		
10.470	84 445	5.891	10.473		
[10.579][a]	85 325	6.934	10.578		
[10.642][a]	85 833	7.864	10.645		
		5. 2e → nf(nde)			
		Part (a)			
9.038	72 896	3.006	9.040		72 957[c]
9.706	78 195	4.022	9.697		78 157
10.000	80 658	5.007	10.002		
[10.165][a]	81986	5.999	10.167		
-	-	-	-		
-	-	-	-		
10.380	83 720	9.136	10.376		
10.408	83 946	10.039	10.407		
(10.435)[b]	84 164	11.224	10.431		
		Part (b)			
[9.352]	[75 429]	[3.002]			
10.018	80 801	4.015	10.018		80 758
10.319	83 228	5.006	10.321		
[10.579]	85 398	7.047	10.585		

Assignments, effective quantum numbers and energies E_{Fit} resulting from the fit to Eq. (5) are included. For the error estimated on the present data, see text. (1 eV = 8065.545 cm^{-1} [34]).

[a] Data in square brackets: at least two possible assignments. For explanation see text.

[b] Data in parentheses correspond to very weak signals.

[c] Alternative assignments of foreign data.

Published in: Chemical Physics (2005), vol. 317, pp. 73-86
Status: Postprint (Author's version)

. Fig. 4(a) and (b) show the correlation of ln T_n as a function of ln(n) for the 2e → nsa$_1$ and the 2e → npa$_1$ transitions in CH_3Br and Kr. For the atomic states we chose the ($^2P_{3/2}$)nℓ and the ($^2P_{1/2}$)nℓ' Rydberg states. Within the manifold thus obtained the term value closest to that measured in CH_3Br is selected. J is no longer a good quantum number. By this way, most of the data overlap and this observation is a good support for the assignments proposed in the present work.

Table 2 reports 2e → npe transitions for Rydberg series converging to the $^2E_{3/2}$ and $^2E_{1/2}$ ionic states. They start at 8.335 eV (67 226 cm^{-1}) and 8.684 eV (70 041 cm^{-1}), respectively. These type of transitions were not considered in both reports of Hochmann et al. [24] and Causley and Russell [26]. In the latter work two transitions, i.e. at 8.337 eV (67 246 cm^{-1}) and 8.689 eV (70 083 cm^{-1}), were assigned to a vibronic transition (noticed by v_2') in the ($^2E_{3/2}$)5p Rydberg state and to a 2e → 5d transition, respectively.

Like for the npa$_1$ series, both series could nearly be characterized by a single average quantum defect δ = 0.543 ± 0.024 and 0.533 ± 0.028 when Eq. (1) is used to fit the data. The 70 161 cm^{-1} [24] and the 70 083 cm^{-1} [26] transitions (shown in brackets in Table 2) fit in these series whereas the transition at 67 304 cm^{-1} [24] is compatible with the line observed at 67 226 cm^{-1} in the present work and assigned to 2e → 5pe converging to $^2E_{3/2}$.

Fig. 4. *Correlation diagrams of ln(T_n) as a function of ln(n) for s- (a), p- (b), d- (c) and f-type (d) transitions in Kr and CH_3Br.*

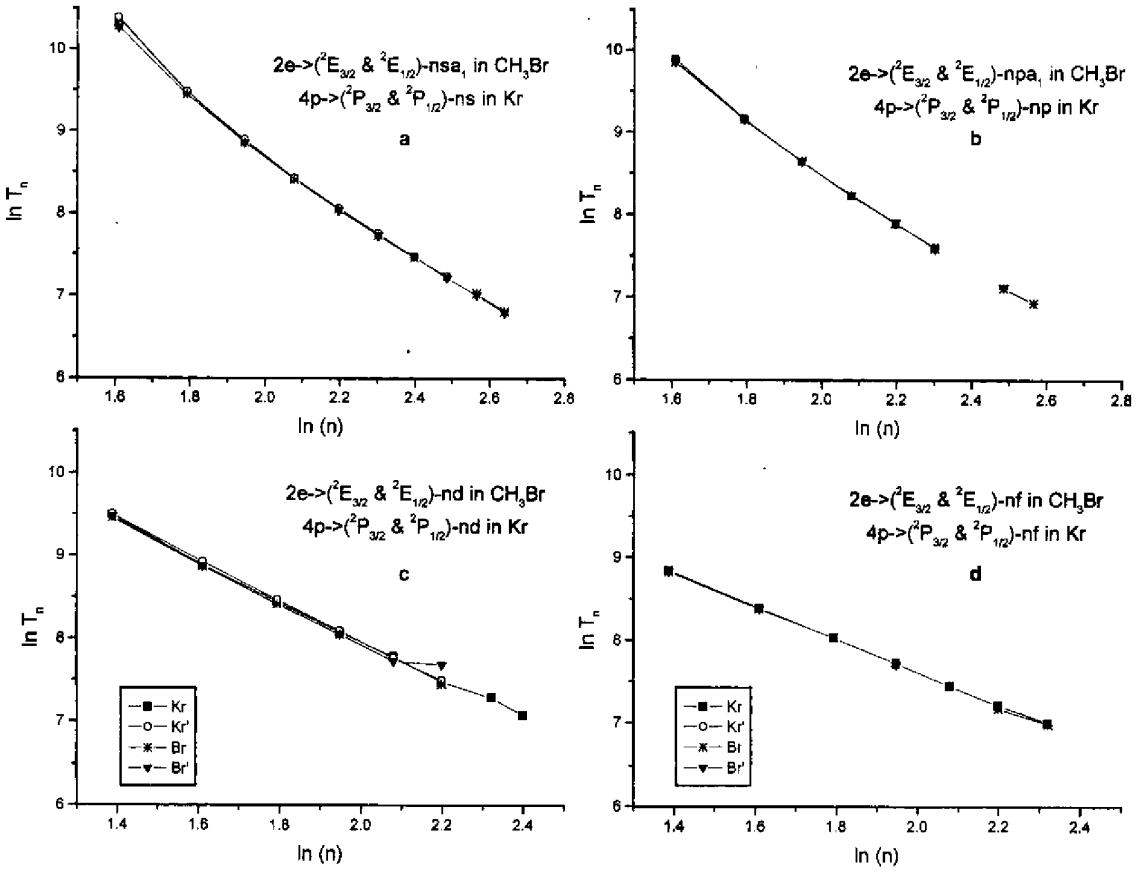

At this point it has to be stressed that (i) the variation of δ with n is as random as observed for the nsa$_1$ Rydberg series and (ii) the averaged quantum defects of the npa$_1$ and npe Rydberg states in CH_3Br, i.e. $\delta \approx 0.58$ and $\delta \approx 0.54$, respectively, are much closer than in the case of CH_3Cl where the corresponding values are δ = 0.67 and δ = 0.43 [7]. This indicates that the quantum defect associated with these orbitals both converge to the typical value $\delta \approx 0.5$ for np-type Rydberg orbitals. These become less discernible as the atomic number of the heteroatom increases, converging to a nearly "atomic" situation.

Hochmann et al. [24] and Causley and Russell [26] identified 2e → nd and 2e → nd' transitions to Rydberg states converging to the $^2E_{3/2}$ and $^2E_{1/2}$ ionic states as already mentioned and shown in Table 2. Surprisingly, the former authors associated effective quantum numbers of 2.49 and 2.51 to these transitions. On

the other hand, the latter tentatively assigned the 70 083 cm^{-1} and the 72 957 cm^{-1} lines to nd and nd' transitions. They argued by the near equality of the term values associated with these transitions and those measured in the Kr atom.

In the present work twelve transitions starting at 8.947 eV (72 162 cm^{-1}) and at 9.256 eV (74 655 cm^{-1}) could be associated with low quantum defect values equal on average to δ — 0.076 ± 0.018 and 0.085 ± 0.035. A reasonable interpretation is to assign them to nd series converging to the $^2E_{3/2}$ and $^2E_{1/2}$ ionic states. For these same transitions, Fig. 4(c) shows a fairly good correlation between ln T_n for the 2e → nd transitions and the corresponding transitions in the Kr atom.

Furthermore, a number of lines could be characterized by a very low value of the quantum defect, i.e. $\delta \leq 0.00$, and clearly distinct from the nd series identified previously. They can be assigned to 2e → nf Rydberg transitions on the basis of (i) the low and even negative δ value and (ii) the good correlation between the present results and those related to Kr in the ln T_n diagram shown in Fig. 4(d).

However, an alternative interpretation is possible for one or both series. As for the p series, the non-sphericity of the ionic core induces a splitting of the d series into one a_1 series and two e series. The series corresponding to a very low quantum defect could be assigned to one of these d series.

Only Causley and Russell [26] assigned the 78 157 cm^{-1} band on the basis of its term value. This line is assigned to a 2e → 5f transition measured at 78 195 cm^{-1} in the present work and corresponding to a 2e → 6f transition. The nf series should indeed start at 9.038 eV (72 896 cm^{-1}) which agrees fairly well with the line reported at 72 957 cm^{-1} [26] and which is assigned to a 2e → 5d transition by these authors. Finally, a short Rydberg series starting at 10.018 eV (80 801 cm^{-1}) has been assigned to 2e → nf transitions to Rydberg states converging to the $^2E_{1/2}$ ionic state. This energy is in good agreement with the line reported earlier at 80 758 cm^{-1} [26].

To find a support to this interpretation of the CH_3Br photoabsorption spectrum, we measured the corresponding data for CD_3Br whose spectrum is reproduced in Fig. 3 between 6 and 12 eV photon energy. The transition energies are listed in Table 3.

Before any assignment can be made by using the Rydberg formula (1), the values of the ionization limits and those of the quantum defects are required. The former quantity has been measured by photo-electron spectroscopy. The He(I) photoelectron spectrum of CD_3Br^+ ($\tilde{X}\,^2E$) band has been recorded with 1 meV increments over 1024 channels. A mixture of Ar/Kr/Xe is introduced simultaneously for electron energy scale calibration. The lowest ionization energies, i.e. $IE_{ad}(\tilde{X}\,^2E_{3/2})$ = 10.565 ±0.004 eV and $IE_{ad}(\tilde{X}\,^2E_{1/2})$ = 10.902 ± 0.004 eV have been determined with respect to the three rare gas ions doublets [32]. These two values of the convergence limits will be used throughout for the analysis of the CD_3Br photoabsorption spectrum.

A long Rydberg series is observed for the 2e → nsai transitions, where the principal quantum number n — 5-16 is observed for both series converging respectively to $\tilde{X}\,^2E_{3/2}$ [part (a) in Table 3] and $\tilde{X}\,^2E_{1/2}$ [part (b) in Table 3]. For both components the quantum defects δ = 1.077 and δ = 1.070 are determined, as averaged over about 11 transitions.

The only known UV spectroscopic work on CD_3Br has been reported by Felps et al. [22], but this study was limited to the 151-180 nm (55 550-66 220 cm^{-1}) spectral region. In this range two vibrationless Rydberg transitions take place, i.e. at 56 285 and 59 255 cm^{-1} [22] which have to be compared with 56 305 and 59 282 cm^{-1} measured in this work (see Table 3). The comparison between the data for the non-deuterated and the deuter-ated species provides us with stronger support for the proposed assignments in CH_3Br.

As is the case of CH_3Br, the photoabsorption spectrum of CD_3Br shows long 2e → npa_1 and 2e → npe series converging to both $^2E_{3/2}$ and $^2E_{1/2}$ spin-orbit components of the ground ionic state. For the npa_1 series, transitions are partially observed between n = 5-22. The 2e → npe is shorter and is detected up to n = 13. Averaged quantum defects δ = 0.58 and δ = 0.62, compared to 0.59 and 0.58 in CH_3Br, are observed for the npa_1 series. For the npe series the corresponding values are δ = 0.50 and δ = 0.53 (compared to 0.54 and 0.53 for CH_3Br).

Contrarily to the CH_3Br spectrum, the 2e → nd transitions in CD_3Br give rise to longer and better defined Rydberg series characterized by average quantum defects δ = 0.080 and δ = 0.147. The corresponding quantities in CH_3Br were found to be δ = 0.076 and 0.085. The fairly good agreement between these values tends to support the classification and assignments suggested for the Rydberg lines in the spectrum of CH_3Br (see Table 2).

Published in: Chemical Physics (2005), vol. 317, pp. 73-86
Status: Postprint (Author's version)

Table 3 *: Vibrationless Rydberg transitions as observed in CD_3Br in the present work for both spin-orbit components: parts (a) and (b) converge to the $^2E_{3/2}$ and $^2E_{1/2}$ ionic states, respectively*

E_{Ryd} (eV)	E_{Kyd} (cm^{-1})	n^*	E_{fit}(eV)
	1. 2e → nsa$_1$		
	Part (a)		
6.981	56 305	1.948	6.983
9.019	72 743	2.967	9.004
9.699	78 227	3.964	9.694
10.003	80 720	4.942	10.010
10.173	82 067	5.891	10.181
10.275	82 873	6.849	10.284
[10.347]	83 446	7.882	10.345
10.392	83 817	8.868	10.395
10.430	84 124	(10.039)	10.428
10.452	84 301	10.973	10.452
10.470	84 446	11.967	10.470
10.480	84 527	(12.652)	10.484
Part (b)			
7.350	59 282	1.957	7.351
9.341	75 340	2.952	9.343
10.040	80 978	3.973	10.032
[10.347]	83 454	4.951	10.347
10.513	84 793	5.914	10.518
10.628	85 721	7.047	10.621
[10.684]	86 172	7.900	10.687
[10.730]	86 543	8.894	10.732
[10.786]	86 995	10.830	10.789
10.807	87 164	11.967	10.807
	2. 2e → npa$_1$		
Part (a)			
8.201	66 150	2.399	8.198
9.401	75 824	3.419	9.386
9.867	79 583	4.415	9.861
10.097	81438	5.392	10.098
10.230	82 510	6.373	10.233
10.315	83 196	7.377	10.316
[10.412][a]	83 978	9.430	10.410
[10.437][a]	84 180	10.310	10.439
[10.459][a]	84 358	11.329	10.460
[10.501][a]	84 696	14.580	10.499
[10.509][a]	84 761	15.587	10.508
[10.520][a]	84 850	17.388	10.520
[10.529][a]	84 922	19.441	10.529
	Part (b)		
8.526	68 767	2.393	8.535
9.726	78 445	3.401	9.723
10.194	82 220	4.384	10.198
10.431	84 131	5.375	10.435
10.568	85 237	6.382	10.570
10.709	86 374	8.396	10.708
10.746	86 672	9.339	10.748
10.775	86 906	10.350	10.776

(continued on next page

Published in: Chemical Physics (2005), vol. 317, pp. 73-86
Status: Postprint (Author's version)

Table 3 *(continued)*

E_{Ryd} (eV)	E_{Ryd} (cm^{-1})	n^*	E_{fit}(eV)
	3. 2e → npe		
	Part (a)		
8.318	68 089	2.461	8.314
9.431	76 066	3.464	9.427
9.878	79 621	4.450	9.880
10.113	81 567	5.486	10.108
10.243	82 615	6.500	10.239
10.324	83 269	7.513	10.320
10.379	83 712	8.553	10.375
[10.412/.417][a]	83 978	9.430	10.413
-	-	-	-
-	-	-	-
-	-	-	-
-	-	-	-
[10.501][a]	84 696	14.580	10.500
[(10.509)][a,b]	84 761	15.587	10.508
-	-	-	-
-	-	-	-
(10.529)[b]	84 922	19.441	10.529
	Part (b)		
8.643	69 711	2.454	8.651
9.770	78 800	3.467	9.764
10.215	82 390	4.450	10.217
10.574	85 285	6.440	10.576
10.716	86 430	8.552	10.715
10.750	86 705	9.461	10.750
10.777	86 922	10.433	10.777
	4. 2e → nd(a_1)		
Part (a)			
9.678	78 058	3.917	9.677
10.003	80 680	4.920	10.002
10.174	82 058	5.899	10.176
10.278	82 898	6.885	10.280
[10.347][a]	83 454	7.900	10.348
[10.392][a]	84 817	8.868	10.394
[10.452][a]	84 301	10.973	10.451
[10.470][a]	84 446	11.967	10.469
[10.484][a]	84 559	12.960	10.483
	Part (b)		
9.996	80 623	3.875	10.014
10.334	83 349	4.894	10.339
[10.617][a]	85 632	6.909	10.617
[10.684][a]	86 172	7.900	10.685
[10.730][a]	86 543	8.894	10.731
[10.762][a]	86 801	9.858	10.764
[10.786][a]	86 995	10.877	10.788
10.804	87 140	11.783	10.806
10.819	87 261	12.803	10.820
[10.831][a]	87 358	13.843	10.832
	5. 2e → nf(nde)		
	Part (a)		
9.716	78 364	4.003	9.710
10.021	80 825	5.001	10.018

(continued on next page)

Published in: Chemical Physics (2005), vol. 317, pp. 73-86
Status: Postprint (Author's version)

Table 3 *(continued)*

E_{Ryd} (eV)	E_{Ryd} (cm^{-1})	n^*	E_{Fit} (eV)
10.191	82 196	6.031	10.185
10.286	82 962	6.983	10.286
10.397	83 857	8.999	10.397
10.431	84 132	10.071	10.429
[10.452][a]	84 301	10.973	10.452
[10.470][a]	84 446	11.967	10.470
[10.484][a]	84 559	12.960	10.484
-	-	-	-
-	-	-	-
10.511	84 777	15.873	10.511
	Part (b)		
10.016	80.784	3.919	10.047
10.339	83 390	4.916	10.356
[10.513][a]	84 793	5.914	10.523
[10.617][a]	85 632	6.909	10.623
[10.684][a]	86 172	7.900	10.689
[10.730][a]	86 543	8.894	10.734
[10.762][a]	86 801	9.858	10.766
[10.786][a]	86 995	10.877	10.789
[10.807][a]	87 167	11.967	10.807
10.821	87 277	12.960	10.821
[10.831][a]	87 358	13.843	10.832

Assignments, effective quantum numbers and energies E_{Fit} resulting from the fit to Eq. (5) are included (1 eV = 8065.545 cm^{-1} [34]).
[a] Data in square brackets: at least two possible assignments. For explanation see text.
[b] Data in brackets: weak signals.

On the basis of the low and often negative values of δ, Table 3 shows at least a series of 9 to 10 lines which consistently pertain to nf-type Rydberg series or to another d series converging to the $^2E_{3/2}$ ionic state. The series converging to $^2E_{1/2}$ is much less certain because it overlaps to a large extent the other 2e→ nd series.

4.4. The low energy region: Exchange versus spin-orbit interactions

In the low n regime, the $(2e)^3(nla_1)$ configuration leads to a ^3E and a ^1E states, which are separated by an interval equal to $2K$ where K is the exchange integral. When the spin-orbit coupling is switched on, the ^3E state is further split into two E states, one A_1 state and one A_2 state. If the C_{3v} field for these Rydberg states is approximated as nearly cylindrical ($C_{\infty v}$), then the projection of the total electronic angular momentum on the cylinder axis is a constant of motion. One of the E states deriving from the ^3E corresponds to $\Omega = 2$, the other one to $\Omega = 1$, whereas $\Omega = 1$ applies for the ^1E. When n increases the singlet-triplet splitting decreases as $(n^*)^{-3}$ so that the spin-orbit coupling constant A becomes comparable with K. The spin-orbit operator H^{so} is able to couple the ^1E ($\Omega = 1$) and ^3E ($\Omega = 1$) substrates. Their mixing increases with n to reach eventually a 1:1 ratio corresponding to Hund's case (c). In this latter regime, two series with the same quantum defect should converge respectively to CH_3Br^+ $\tilde{X}\,^2E_{3/2}$ and $\tilde{X}\,^2E_{1/2}$.

Out of the 5 states corresponding to the $(2e)^3(nla_1)$ configuration, the dipolar transition probability from the ground state $\tilde{X}\,^1A_1$ of CH_3Br will be shared between both $\Omega = 1$ states with an intensity ratio governed by the K/A ratio. In pure Hund's case (c) the intensity ratio is equal to 1. In pure Hund's case (a), the transition to ^3E is forbidden.

In Hund's case (a) the Rydberg states energies are given by Eqs. (2) and (3):

$$E' = E(^3E) = \bar{E}^{ion}_{^2E} - \frac{R}{(n-\delta')^2}, \qquad (2)$$

$$E'' = E(^1E) = \bar{E}^{ion}_{^2E} - \frac{R}{(n-\delta'')^2}, \qquad (3)$$

where $\bar{E}^{ion}_{2E}$ is the ionization energy which would be observed if the spin-orbit coupling were absent. In practice,

it is the average ionization energy as defined by

$$\bar{E}^{\text{ion}}_{^2E} = \frac{1}{2}\left[E^{\text{ion}}_{^2E_{3/2}} + E^{\text{ion}}_{^2E_{1/2}}\right]. \qquad (4)$$

Table 4 *: Calculated quantum defects δ′ and δ″ obtained by fitting Eq. (5) to the data related to the nsa_1, npa_1, npe, nd and nf series in CH_3Br and CD_3Br, standard deviation (σ) between the experimental and fitted energies (meV) and values of the exchange coupling element K for n = 3 in meV (cm^{-1})*

	nsa_1	**npa_1**	**npe**	**nd**	**nf**
			CH_3Br		
δ′	1.076	0.616	0.552	-0.0003	0.025
δ″	1.016	0.579	0.470	-0.0006	-0.053
σ	4	3	6	8	6
K(n = 3)	110(887)	36 (290)	72 (581)	<0.2 (1.6)	39 (314)
			CD_3Br		
δ′	1.067	0.603	0.542	0.085	0.010
δ″	1.026	0.603	0.542	0.085	0.010
σ	6	4	3	5	9
K(n = 3)	75 (605)				

As the triplet state is more stable than the singlet, *δ′)δ″*.

Eq. (5) below is valid in the whole coupling range. It takes into account both exchange and spin-orbit interactions.

$$E = \frac{E' + E''}{2} \pm \sqrt{\left(\frac{E' - E''}{2}\right)^2 + A^2}$$
$$= \frac{E' + E''}{2} \pm \sqrt{K^2 + A^2}. \qquad (5)$$

Eq. (5) reduces to Hund's case (a) when $K >> A$ (small *n)* and to Hund's case (c) when $K << A$ (large *n)*. In this latter case, inserting (2) and (3) into (5) and expanding in powers of n^{-1} leads to two Rydberg series:

$$E^{+} = E^{\text{ion}}_{^2E_{1/2}} - \frac{R}{(n - \bar{\delta})^2}, \qquad (6)$$

$$E^{-} = E^{\text{ion}}_{^2E_{3/2}} - \frac{R}{(n - \bar{\delta})^2}, \qquad (7)$$

with $\bar{\delta}$ = (*δ′* + *δ″*)/2. Two series with the same average quantum defect converge to the two spin-orbit components of the ionic state.

We fitted the energies of all the observed Rydberg series to Eq. (5) by assuming no *n* variation of the *δ′* and *δ″* quantum defects. The spin-orbit coupling constant *A* has been taken as half the ionic $^2E_{3/2}$-$^2E_{1/2}$ splitting, i.e. 159.5 meV [30] for CH_3Br^+ and 168.5 meV for CD_3Br^+ [32]. The fitted energies (labeled as E_{fit}*)* are listed in Tables 2 and 3. Table 4 summarizes the results.

At this point some aspects have to be stressed, (i) The fit of Eq. (5) with constant quantum defects, i.e. with only two free parameters, seems appropriate to account for most of the experimental data, (ii) We attempted to apply the same treatment to all transition types, i.e. nsa_1, npa_1, npe, nd and nf. The coupling scheme seems to hold for all these transitions at least in CH_3Br. (iii) Already for *n* = 6, CH_3Br and CD_3Br behave as pure Hund's case (c)-systems. This would likely be the reason why only tiny differences exist between the fittings by Eq. (5) and its simplified form Eq. (1). (iv) Quite surprisingly, the $^3E_1$-$^1E_1$ coupling constant *K* shows a non-negligible change with isotopic substitution. For $5sa_1$ the constant *K* is equal to 110 meV in CH_3Br whereas *K*= 75 meV in CD_3Br. This effect is not observed in CH_3C1 and CD_3C1 where *K*= 55 and 56 meV, respectively, for $3sa_1$ [7]. This could be due to vibronic interactions in spite of the small-ness of the Jahn-Teller coupling.

5. Conclusions

The vacuum UV photoabsorption spectrum of CH_3Br has been reexamined in detail between 6 and 25 eV photon energy at medium resolution. A few weak diffuse absorption bands have been observed in the 12-24 eV photon energy range. These were essentially assigned to 3 s Rydberg states, members of series converging to $3a_1^{-1}$, $1e^{-1}$, and higher ionization limits. Very likely many electron transitions are involved in the bands observed above 18.0 eV [27, 35].

In the 6-12 eV photon energy range, both in CH_3Br and CD_3Br, as observed at medium and high resolution, many lines spread between 7 and 10.8 eV and are assigned to Rydberg series converging to the spin-orbit split $\tilde{X}\,^2E_{3/2}$-$^2E_{1/2}$ ground state of CH_3Br^+. Vibration-less Rydberg transitions have been classified on the basis of their quantum defect δ.

First, using the simple Rydberg formula, δ is observed to be reasonably constant for one orbital-type transition. Five Rydberg series for each spin-orbit component have been detected: nsa_1 (δ = 1.067 and 1.032), npa_1 (δ = 0.588 and 0.579), npe (δ = 0.543 and 0.533), nd (δ = 0.076 and 0.085) and nd and/or nf (δ = -0.047 and -0.023).

To confirm the present interpretation, the photoabsorption spectrum of CD_3Br has been analyzed for the first time. Assignments were made by the same procedure. Also in this molecule the quantum defects remain fairly constant for one orbital-type transition. It has been noticed that its value for npa_1 (δ = 0.58 and 0.62) and for npe (δ = 0.50 and 0.53) are very close, as observed in CH_3Br also. This is in contrast to our observations in CH3Cl [7]. The isotopic shift on the vibronic transition allowed us to observe longer nd and nf series. In a second step, the combined effects of the exchange interaction, leading to singlet-triplet splitting, and of the spin-orbit coupling are considered. Good quality fits of Eq. (5) to the experimental data could be obtained with constant quantum defects in the whole observed n range. Already Rydberg states with n = 6 correspond to pure Hund's case (c).

Acknowledgements

We are indebted to the University of Liège, the Freie Universität Berlin and the Bundesministerium fur Fors-chung und Technologie for financial support. R.L. and B.L. gratefully acknowledge the European Community for its support through its TMR programme (Contract EU-HPRI-1999CT-00028). H.B. acknowledges the Fonds den Chemischen Industrie for financial support. The generous financial support of the Direction de la Recherche Scientifique de la Communauté Française de Belgique through an Action de Recherche Concertée (A.R.C.) is gratefully acknowledged. We would finally acknowledge Dr. Gert Reichardt for his kindness and always very precious experience in maintaining the 3m-NIM monochromator in the best operating conditions.

References

[1] O.N. Sing, P. Fabian, in: P. Febian, O.N. Singh (Eds.), Reactive Bromine compounds in The Handbook of Environmental Chemistry. Part 4E: Reactive Halogen Compounds in the Atmosphere, Springer Verlag, Berlin, 1999, p. 3.

[2] S.A. Montzka, P.J. Fraser, Controlled substances and other source gases, in: A.N. Ajevon, D.L. Albritton, G. Mégie, R. Watson (Ed.), Scientific Assessment of Ozone Depletion: 2002, Global Ozone Research and Monitoring Project, Rep. No. 47, World Meteorological Organization, Geneva, 2003 (Chapter 1).

[3] R. Locht, J. Momigny, Int. J. Mass Spectrom. Ion Proc. 71 (1986) 141.

[4] R. Locht, E. Rühl, J. Momigny, H. Baumgärtel, Chem. Phys. 117 (1987) 305.

[5] R. Locht, J. Momigny, in: F. Lahmani (Ed.), Photophysics and Photochemistry above 6 eV, Elsevier, Amsterdam, 1985, p. 171.

[6] R. Locht, B. Leyh, A. Hoxha, D. Dehareng, H.W. Jochims, H. Baumgartel, Chem. Phys. 257 (2000) 283.

[7] R. Locht, B. Leyh, A. Hoxha, H.W. Jochims, H. Baumgärtel, Chem. Phys. 272 (2001) 259.

[8] R. Locht, B. Leyh, A. Hoxha, D. Dehareng, H.W. Jochims, H. Baumgärtel, Chem. Phys. 272 (2001) 277.

[9] R. Locht, B. Leyh, A. Hoxha, D. Dehareng, K. Hottmann, H.W. Jochims, H. Baumgärtel, Chem. Phys. 272 (2001) 293.

[10] J. Momigny, R. Locht, Chem. Phys. Lett. 211 (1993) 161.

[11] R. Locht, B. Leyh, K. Hottmann, H. Baumgärtel, Chem. Phys. 220 (1997) 217.

[12] R. Locht, B. Leyh, K. Hottmann, H. Baumgärtel, Chem. Phys. 220 (1997) 229.

[13] A. Hoxha, R. Locht, B. Leyh, D. Dehareng, K. Hottmann, H. Baumgärtel, Chem. Phys. 256 (2000) 239.

[14] A. Hoxha, R. Locht, B. Leyh, D. Dehareng, K. Hottmann, H.W. Jochims, H. Baumgärtel, Chem. Phys. 260 (2000) 237.

[15] A. Hoxha, R. Locht, A.J. Lorquet, J.C. Lorquet, B. Leyh, J. Chem. Phys. 111 (1999) 9259.

[16] K.M. Weitzel, F. Güthe, J. Mähnert, R. Locht, H. Baumgärtel, Chem. Phys. 201 (1995) 287.

[17] F. Güthe, R. Locht, B. Leyh, H. Baumgärtel, K.M. Weitzel, J. Phys. Chem. A 103 (1999) 8404.

[18] W. Zhang, G Cooper, T. Ibuki, CE. Brion, Chem. Phys. 137 (1989) 391, and references therein.

[19] W. Zhang, G Cooper, T. Ibuki, CE. Brion, Chem. Phys. 151 (1991) 343, and references therein.

[20] W. Zhang, G Cooper, T. Ibuki, CE. Brion, Chem. Phys. 153 (1991) 491, and references therein.

[21] J.W. Au, GR. Barton, CE. Brion, Chem. Phys. 221 (1997) 151, and references therein.

[22] S. Felps, P. Hochmann, P. Brint, S.P. McGlynn, J. Mol. Spectrosc. 59 (1976) 355.

[23] W.C. Price, J. Chem. Phys. 4 (1936) 539.

[24] P. Hochmann, P.H. Templet, H.T. Wang, S.P. McGlynn, J. Chem. Phys. 62 (1975) 2588.

[25] W.S. Felps, K. Rupnik, S.P. McGlyn, J. Phys. Chem. 95 (1991) 639.

[26] G.C. Causley, B.R. Russell, J. Chem. Phys. 62 (1975) 848.

[27] T.N. Olney, G Cooper, W.F. Chan, GR. Burton, CE. Brion, K.H. Tan, Chem. Phys. 218 (1997) 127.

[28] G Reichardt, T. Noll, I. Packe, P. Rotter, J.-S. Schmidt, W. Gudat, Nucl. Instr. and Meth. A 467-468 (2001) 458.

[29] R. Locht, B. Leyh, W. Denzer, G Hagenow, H. Baumgartel, Chem. Phys. 155 (1991) 407.

[30] L. Karlsson, R. Jadrny, L. Mattsson, F.T. Chau, K. Siegbahn, Phys. Scripta 16 (1977) 225.

[31] W. Von Niessen, L. Asbrink, G Bieri, J. Electr. Spectr. Rel. Phennom. 26 (1982) 173.

[32] R. Locht, E. Gridelet, B. Leyh, D. Dehareng, to be published.

[33] T.N. Olney, W.F. Chan, G Cooper, CE. Brion, K.H. Tan, J. Electr. Spectr. Rel. Phenom. 66 (1993) 83.

[34] P.J. Mohr, B.N. Taylor, J. Phys. Chem. Ref. Data 28 (1999) 1713.

[35] R. Locht, B. Leyh, K. Hottmann, H.W. Jochims, H. Baumgärtel, to be published.

[36] CE. Moore, Atomic energy levels, vol. II, Circ. 467, US Department of Commerce, N.B.S., Washington, DC, 1949.